Micro-Doppler Effect in Radar: Phenomenon, Model, and Simulation Study

VICTOR C. CHEN
Naval Research Laboratory

FAYIN LI

SHEN-SHYANG HO

HARRY WECHSLER, Fellow, IEEE
George Mason University

When, in addition to the constant Doppler frequency shift induced by the bulk motion of a radar target, the target or any structure on the target undergoes micro-motion dynamics, such as mechanical vibrations or rotations, the micro-motion dynamics induce Doppler modulations on the returned signal, referred to as the micro-Doppler effect. We introduce the micro-Doppler phenomenon in radar, develop a model of Doppler modulations, derive formulas of micro-Doppler induced by targets with vibration, rotation, tumbling and coning motions, and verify them by simulation studies, analyze time-varying micro-Doppler features using high-resolution time-frequency transforms, and demonstrate the micro-Doppler effect observed in real radar data.

Manuscript received March 1, 2003; revised July 1, 2004 and March 3, 2005; released for publication August 5, 2005.

IEEE Log No. T-AES/42/1/870577.

Refereeing of this contribution was handled by L. M. Kaplan.

This work was supported in part by the Office of Naval Research and the Missile Defense Agency.

Authors' addresses: V. C. Chen, Radar Division, Naval Research Laboratory, Code 5311, 4555 Overlook Ave. SW, Washington, D.C. 20375; F. Li, S-S. Ho, and H. Wechsler, Dept. of Computer Science, George Mason University, Fairfax, VA 22030.

I. INTRODUCTION

When a radar transmits an electromagnetic signal to a target, the signal interacts with the target and returns back to the radar. Changes in the properties of the returned signal reflect the characteristics of interest for the target. When the target moves with a constant velocity, the carrier frequency of the returned signal will be shifted. This is known as the Doppler effect [1]. For a mono-static radar where the transmitter and the receiver are at the same location, the roundtrip distance traveled by the electromagnetic wave is twice the distance between the transmitter and the target. The Doppler frequency shift is determined by the wavelength of the electromagnetic wave and the relative velocity between the radar and the target: $f_D = -2\lambda V$, where $\lambda = c/f$ is the wavelength and V is the relative velocity. If the radar is stationary, the relative velocity V will be the velocity of the target along the line of sight (LOS) of the radar, known as the radial velocity. When the target is moving away from the radar, the velocity is defined to be positive, and as a consequence the Doppler shift is negative.

If the target or any structure on the target has mechanical vibration or rotation in addition to its bulk translation, it might induce a frequency modulation on the returned signal that generates sidebands about the target's Doppler frequency shift. This is called the micro-Doppler effect [2–4]. Radar signals returned from a target that incorporates vibrating or rotating structures, such as propellers of a fixed-wing aircraft, rotors of a helicopter, or the engine compressor and blade assemblies of a jet aircraft, contain micro-Doppler characteristics related to these structures. The micro-Doppler effect enables us to determine the dynamic properties of the target and it offers a new approach for the analysis of target signatures. Micro-Doppler features serve as additional target features that are complementary to those made available by existing methods. The micro-Doppler effect can be used to identify specific types of vehicles, and determine their movement and the speed of their engines. Vibrations generated by a vehicle engine can be detected by radar signals returned from the surface of the vehicle. From micro-Doppler modulations in the engine vibration signal, one can distinguish whether it is a gas turbine engine of a tank or the diesel engine of a bus.

The micro-Doppler effect was originally introduced in coherent laser systems [3]. A coherent laser radar system transmits electromagnetic waves at optical frequencies and receives the backscattered light waves from targets. A coherent system preserves the phase information of the scattered waves with respect to a reference wave and has greater sensitivity to any phase variation. Because a half-wavelength change in range can cause a 360° phase change, for a coherent laser system with a wavelength of $\lambda = 2$ μm, 1 μm

variation in range would cause a 360° phase change.

In many cases, a target or a structure on the target may have micro-motions, such as vibrations or rotations. The source of rotations or vibrations might be a rotating rotor of a helicopter, a rotating antenna on a ship, mechanical oscillations in a bridge or a building, an engine-induced vibrating surface, or other causes. Micro-motion dynamics produce frequency modulations on the back-scattered signal and would induce additional Doppler changes to the constant Doppler frequency shift of the bulk translational motion. For a target that has only translation with a constant velocity, the Doppler frequency shift induced by translation is a time-invariant function. If the target also undergoes a vibration or rotation, then the Doppler frequency shift generated by the vibration or rotation is a time-varying frequency function and imposes a periodic time-varying modulation onto the carrier frequency. Micro-motions yield new features in the target's signature that are distinct from its signature in the absence of micro-motions.

For a pure periodic vibration or rotation, micro-motion dynamics generate sideband Doppler frequency shifts about the Doppler shifted central carrier frequency. The modulation contains harmonic frequencies that depend on the carrier frequency, the vibration or rotation rate, and the angle between the direction of vibration, and the direction of the incident wave. Because the frequency modulation is a phase change in the signal, in order to extract useful information from the modulation, coherent processing must be used to carefully track the phase change.

For a vibration scatterer, if the vibration rate in angular frequency is ω_v and the maximal displacement of the vibration is D_v, the maximum Doppler frequency variation is determined by $\max\{f_D\} = (2/\lambda)D_v\omega_v$. As a consequence, for very short wavelengths, even with very low vibration rate ω_v any micro vibration of D_v can cause large phase changes. As a consequence the micro-Doppler frequency modulation or the phase change with time can be easily detected. A coherent laser radar operating at 1.5 μm wavelength, can achieve a velocity precision ΔV better than 1 mm/s, or a Doppler resolution of $\Delta f_D = 2\Delta V/\lambda = 1.33$ KHz.

Because the micro-Doppler effect is sensitive to the operating frequency band, for radar systems operating at microwave frequency bands, the phenomenon may also be observable if the product of the target's vibration rate and the displacement of the vibration is high enough. For a radar operating at X-band with a wavelength of 3 cm, a vibration rate of 15 Hz with a displacement of 0.3 cm can induce a detectable maximum micro-Doppler frequency shift of 18.8 Hz. If the radar is operated at L-band with a wavelength of 10 cm, to achieve the same maximum micro-Doppler shift of 18.8 Hz at the same vibration rate of 15 Hz, the required displacement must be 1 cm, which may be too large in practice. Therefore, at lower radar frequency bands, the detection of the micro-Doppler modulation generated by vibration may not be possible. The micro-Doppler generated by rotations, such as rotating rotor blades, however, may be detectable because of their longer rotating arms and, thus, higher tip speeds. For example, UHF-band (300–1,000 MHz) radar with a wavelength of 0.6 m, when a helicopter's rotor blade rotates with a tip speed of 200 m/s, can induce a maximum micro-Doppler frequency shift of 666 Hz that is certainly detectable.

To analyze time-varying micro-Doppler frequency features, the Fourier transform, which is unable to provide time-dependent frequency information, is not suitable. An efficient method to analyze time-varying frequency features is to apply a high-resolution time-frequency transform.

The contribution of this paper is that 1) a model of the micro-Doppler effect is developed, 2) mathematical formulas of micro-Doppler modulations induced by several typical basic micro-motions are derived and verified by simulation studies, 3) instead of using the conventional Fourier transform, the high-resolution time-frequency transform is used to analyze time-varying micro-Doppler features, and 4) micro-Doppler effect in radar is demonstrated using real radar data. In Section II, we develop a model for analyzing the micro-Doppler effect. In Section III, we briefly introduce high-resolution time-frequency transforms for analyzing time-varying frequency spectrum. In Section IV, we apply the model for analyzing micro-Doppler effect to several typical micro-motions (vibration, rotation, tumbling, and coning) and verify them using simulation studies. In Section V, we demonstrate two examples of micro-Doppler effect in radar observed in real radar data.

II. MICRO-DOPPLER EFFECT INDUCED BY MICRO-MOTION DYNAMICS

The micro-Doppler effect induced by micro-motions of a target or structures on the target can be derived from the theory of electromagnetic back-scattering field. It can be mathematically formulated by augmenting the conventional Doppler effect analysis using micro-motions.

The characteristics of the electromagnetic back-scattering field from a moving or an oscillating target have been studied in both theory and experiment [5–14]. Theoretical analysis indicates that the translation of a target modulates the phase function of the scattered electromagnetic waves. When the target oscillates linearly and periodically, the modulation generates sideband frequencies about the frequency of the incident wave. A far electric field of

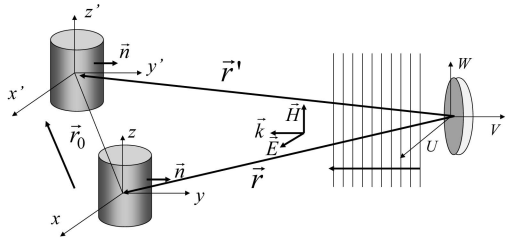

Fig. 1. Geometry of translation target in far EM field.

a translated target can be derived as [8]

$$\vec{E}_T(\vec{r}') = \exp\{jk\vec{r}_0 \cdot (\vec{u}_k - \vec{u}_r)\}\vec{E}(\vec{r}) \tag{1}$$

where $k = 2\pi/\lambda$ is the wave number, $\vec{u}_k$ is the unit vector of the incidence wave, $\vec{u}_r$ is the unit vector of the direction of observation, $\vec{E}(\vec{r})$ is the far electric field of the target before moving, $\vec{r} = (U_0, V_0, W_0)$ is the initial coordinates of the target in the radar coordinates (U,V,W), $\vec{r}' = (U_1, V_1, W_1)$ is the coordinates of the target after translation, and $\vec{r} = \vec{r}' + \vec{r}_0$, where $\vec{r}_0$ is the translation vector, as illustrated in Fig. 1.

From (1) we can see that the only difference in the electric field before and after the translation is the phase factor $\exp\{jk\vec{r}_0 \cdot (\vec{u}_k - \vec{u}_r)\}$. If the translation is a function of time $\vec{r}_0 = \vec{r}_0(t) = r_0(t)\vec{u}_T$, where $\vec{u}_T$ is the unit vector of the translation, the phase factor then becomes

$$\exp\{j\Phi(t)\} = \exp\{jkr_0(t)\vec{u}_T \cdot (\vec{u}_k - \vec{u}_r)\}. \tag{2}$$

For back-scattering, the direction of observation is opposite to the direction of the incidence wave, or $\vec{u}_k = -\vec{u}_r$ and thus

$$\exp\{j\Phi(t)\} = \exp\{j2kr_0(t)\vec{u}_T \cdot \vec{u}_k\}. \tag{3}$$

If the translation direction is perpendicular to the direction of the incidence wave, the phase function is zero and $\exp\{\Phi(t)\} = 1$.

In general, when the radar transmits an electromagnetic wave at a carrier frequency of f, the radar received signal can be expressed as

$$s(t) = \exp\{j2kr_0(t)\vec{u}_T \cdot \vec{u}_k\}\exp\{-j2\pi ft\}|\vec{E}(\vec{r})| \tag{4}$$

where the phase factor, $\exp\{j2kr_0(t)\vec{u}_T \cdot \vec{u}_k\}$, defines the modulation of the micro-Doppler effect caused by the motion $\vec{r}_0(t)$. If the motion is a vibration given by $r_0(t) = A\cos\Omega t$, the phase factor becomes a periodic function of the time with an angular vibrating frequency Ω

$$\exp\{j\Phi(t)\} = \exp\{j2kA\cos\Omega t\vec{u}_T \cdot \vec{u}_k\}. \tag{5}$$

The phase function can be mathematically formulated by introducing micro-motions to augment the conventional Doppler analysis. Let us represent a target as a set of point scatterers that represent the primary scattering centers on the target. The point scattering model simplifies the analysis while preserving the micro-Doppler features. For simplicity, all scatterers are assumed to be perfect reflectors that reflect all the energy intercepted.

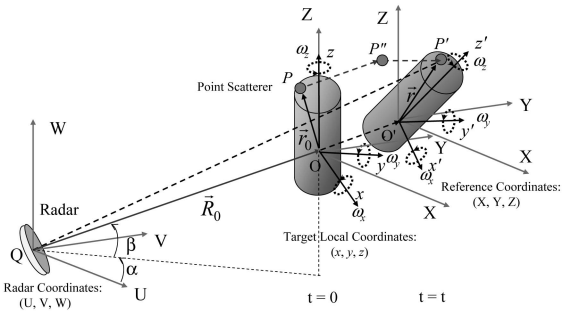

Fig. 2. Geometry of radar and target with translation and rotation.

As shown in Fig. 2, the radar is stationary and located at the origin Q of the radar coordinate system (U,V,W). The target is described in a local coordinate system (x,y,z) attached to it and has translations and rotations with respect to the radar coordinates. To observe the target's rotations, a reference coordinate system (X,Y,Z) is introduced, which shares the same origin with the target local coordinates and, thus, has the same translation as the target but no rotation with respect to the radar coordinates. The origin O of the reference coordinates is assumed to be at a distance R_0 from the radar.

Suppose the target is a rigid body that has translation velocity $\vec{V}$ with respect to the radar and a rotation angular velocity $\vec{\omega}$, which can be either represented in the target local coordinate system as $\vec{\omega} = (\omega_x, \omega_y, \omega_z)^T$, or represented in the reference coordinate system as $\vec{\omega} = (\omega_X, \omega_Y, \omega_Z)^T$. Because the motion of a rigid body can be represented by the position of the body at two different instants of time, a particle P of the body at instant of time $t = 0$ will move to P' at instant of time t. The movement consists of two steps: 1) translation from P to P'', as shown in Fig. 2, with a velocity $\vec{V}$, i.e., $\overrightarrow{OO'} = \vec{V}t$, and 2) rotation from P'' to P' with an angular velocity $\vec{\omega}$. If we observe the movement in the reference coordinate system, the particle P is located at $\vec{r}_0 = (X_0, Y_0, Z_0)^T$, and the rotation from P'' to P' is described by a rotation matrix $\Re_t$. Then, at time t the location of P' will be at

$$\vec{r} = \overrightarrow{O'P'} = \Re_t\overrightarrow{O'P''} = \Re_t\vec{r}_0. \tag{6}$$

The range vector from the radar at Q to the particle at P' can be derived as

$$\overrightarrow{QP'} = \overrightarrow{QO} + \overrightarrow{OO'} + \overrightarrow{O'P'} = \vec{R}_0 + \vec{V}t + \Re_t\vec{r}_0 \tag{7}$$

and the scalar range becomes

$$r(t) = \|\vec{R}_0 + \vec{V}t + \Re_t\vec{r}_0\| \tag{8}$$

where $\|\cdot\|$ represents the Euclidean norm.

If the radar transmits a sinusoidal waveform with a carrier frequency f, the baseband of the signal returned from the particle P as a point scatterer is a function of $r(t)$:

$$s(t) = \rho(x,y,z)\exp\left\{j2\pi f\frac{2r(t)}{c}\right\} = \rho(x,y,z)\exp\{j\Phi[r(t)]\} \quad (9)$$

where $\rho(x,y,z)$ is the reflectivity function of the point scatterer P described in the target local coordinates (x,y,z), c is the speed of the electromagnetic wave propagation, and the phase of the baseband signal is

$$\Phi[r(t)] = 2\pi f\frac{2r(t)}{c}. \quad (10)$$

By taking the time derivative of the phase, the Doppler frequency shift induced by the target's motion is obtained

$$\begin{aligned} f_D &= \frac{1}{2\pi}\frac{d\Phi(t)}{dt} = \frac{2f}{c}\frac{d}{dt}r(t) \\ &= \frac{2f}{c}\frac{1}{2r(t)}\frac{d}{dt}[(\vec{R}_0+\vec{V}t+\Re_t\vec{r}_0)^T(\vec{R}_0+\vec{V}t+\Re_t\vec{r}_0)] \\ &= \frac{2f}{c}\left[\vec{V}+\frac{d}{dt}(\Re_t\vec{r}_0)\right]^T\vec{n} \end{aligned} \quad (11)$$

where $\vec{n} = (\vec{R}_0+\vec{V}t+\Re_t\vec{r}_0)/(\|\vec{R}_0+\vec{V}t+\Re_t\vec{r}_0\|)$ is the unit vector of $\overrightarrow{QP'}$.

To derive the Doppler modulation induced by the rotation, we utilize a useful relationship $\vec{u}\times\vec{r} = \hat{u}\vec{r}$. To prove it, given a vector $\vec{u} = [u_x,u_y,u_z]^T$ define a skew symmetric matrix

$$\hat{u} = \begin{bmatrix} 0 & -u_z & u_y \\ u_z & 0 & -u_x \\ -u_y & u_x & 0 \end{bmatrix}. \quad (12)$$

The cross product of the vector $\vec{u}$ and any vector $\vec{r}$ can be computed through the matrix computation:

$$\vec{u}\times\vec{r} = \begin{bmatrix} u_yr_z-u_zr_y \\ u_zr_x-u_xr_z \\ u_xr_y-u_yr_x \end{bmatrix} = \begin{bmatrix} 0 & -u_z & u_y \\ u_z & 0 & -u_x \\ -u_y & u_x & 0 \end{bmatrix}\begin{bmatrix} r_x \\ r_y \\ r_z \end{bmatrix} = \hat{u}\vec{r}. \quad (13)$$

This relationship is useful in the analysis of the special orthogonal matrix group or SO(3) rotation group, also called the 3D rotation matrix [15].

Now we calculate the rotation matrix in (11). In the reference coordinate system, the angular rotation velocity vector is described by $\vec{\omega} = (\omega_X,\omega_Y,\omega_Z)^T$, and the target will rotate along the unit vector $\vec{\omega}' = \vec{\omega}/\|\vec{\omega}\|$ with a scalar angular velocity $\Omega = \|\vec{\omega}\|$. Assuming a high pulse repetition frequency (PRF) and a relatively low angular velocity, the rotational motion in each small time interval can be considered to be infinitesimal, and thus (see the Appendix)

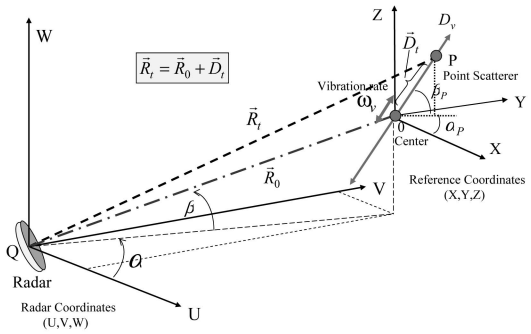

Fig. 3. Geometry for radar and vibrating scatterer.

$$\Re_t = \exp\{\hat{\omega}t\} \quad (14)$$

where $\hat{\omega}$ is the skew symmetric matrix associated with $\vec{\omega}$. Thus, the Doppler frequency shift in (11) becomes

$$\begin{aligned} f_D &= \frac{2f}{c}\left[\vec{V}+\frac{d}{dt}(e^{\hat{\omega}t}\vec{r}_0)\right]^T\vec{n} = \frac{2f}{c}(\vec{V}+\hat{\omega}e^{\hat{\omega}t}\vec{r}_0)^T\vec{n} \\ &= \frac{2f}{c}(\vec{V}+\hat{\omega}\vec{r})^T\vec{n} = \frac{2f}{c}(\vec{V}+\vec{\omega}\times\vec{r})^T\vec{n}. \end{aligned} \quad (15)$$

If $\|\vec{R}_0\| \gg \|\vec{V}t+\Re_t\vec{r}\|$, $\vec{n}$ can be approximated as $\vec{n} = \vec{R}_0/\|\vec{R}_0\|$, which is the direction of the radar LOS. Therefore, the Doppler frequency shift is approximately

$$f_D = \frac{2f}{c}[\vec{V}+\vec{\omega}\times\vec{r}]_{\text{radial}} \quad (16)$$

where the first term is the Doppler shift due to the translation and the second term is the micro-Doppler due to the rotation:

$$f_{\text{micro-Doppler}} = \frac{2f}{c}[\vec{\omega}\times\vec{r}]_{\text{radial}}. \quad (17)$$

A. Vibration-Induced Micro-Doppler Modulation

As shown in Fig. 3, the radar is located at the origin of the radar coordinate system (U,V,W) and a point scatterer P is vibrating about a center point O. The center point is also the origin of the reference coordinate system (X,Y,Z), which is translated from (U,V,W) at a distance R_0 from the radar. We also assume that the center point O is stationary with respect to the radar. If the azimuth and elevation angle of the point O with respect to the radar are α and β, respectively, the point O is located at

$$(R_0\cos\alpha\cos\beta, R_0\sin\alpha\cos\beta, R_0\sin\beta)$$

in the radar coordinates (U,V,W). Then, the unit vector of the radar LOS becomes

$$\vec{n} = [\cos\alpha\cos\beta, \sin\alpha\cos\beta, \sin\beta]^T. \quad (18)$$

Assume that the scatterer P is vibrating at a frequency f_v with an amplitude D_v and that the azimuth and elevation angle of the vibration direction in the reference coordinates (X,Y,Z) are α_P and β_P, respectively. As shown in Fig. 3, the vector from the radar to the scatterer P becomes then $\vec{R}_t = \vec{R}_0 + \vec{D}_t$ and the range of the scatterer P can be expressed as

$$\begin{aligned} R_t = |\vec{R}_t| =& [(R_0\cos\alpha\cos\beta + D_t\cos\alpha_P\cos\beta_P)^2 \\ &+ (R_0\sin\alpha\cos\beta + D_t\sin\alpha_P\cos\beta_P)^2 \\ &+ (R_0\sin\beta + D_t\sin\beta_P)^2]^{1/2}. \end{aligned} \tag{19}$$

When $R_0 \gg D_t$, the range is approximately

$$\begin{aligned} R_t &= \{R_0^2 + D_t^2 + 2R_0D_t[\cos(\alpha-\alpha_p)\cos\beta\cos\beta_p + \sin\beta\sin\beta_p]\}^{1/2} \\ &\approx R_0 + D_t[\cos(\alpha-\alpha_p)\cos\beta\cos\beta_p + \sin\beta\sin\beta_p]. \end{aligned} \tag{20}$$

If the azimuth angle α of the center point O and the elevation angle β_P of the scatterer P are all zero, when $R_0 \gg D_t$ we have

$$\begin{aligned} R_t &= (R_0^2 + D_t^2 + 2R_0D_t\cos\alpha_P\cos\beta)^{1/2} \\ &\cong R_0 + D_t\cos\alpha_P\cos\beta. \end{aligned} \tag{21}$$

Because the vibration rate of the scatterer in angular frequency is $\omega_v = 2\pi f_v$ and the amplitude of the vibration is D_v, $D_t = D_v\sin\omega_v t$ and the range of the scatterer becomes

$$R(t) = R_t = R_0 + D_v\sin\omega_v t\cos\alpha_P\cos\beta. \tag{22}$$

The radar received signal becomes then

$$\begin{aligned} s_R(t) &= \rho\exp\left\{j\left[2\pi ft + 4\pi\frac{R(t)}{\lambda}\right]\right\} \\ &= \rho\exp\{j[2\pi ft + \Phi(t)]\} \end{aligned} \tag{23}$$

where ρ is the reflectivity of the point scatterer, f is the carrier frequency of the transmitted signal, λ is the wavelength, and $\Phi(t) = 4\pi R(t)/\lambda$ is the phase modulation function.

Substituting (22) into (23) and denoting $B = (4\pi/\lambda)D_v\cos\alpha_P\cos\beta$, the received signal can be rewritten as

$$s_R(t) = \rho\exp\left\{j\frac{4\pi}{\lambda}R_0\right\}\exp\{j2\pi ft + B\sin\omega_v t\} \tag{24}$$

which can be further expressed by the Bessel function of the first kind of order k:

$$J_k(B) = \frac{1}{2\pi}\int_{-\pi}^{\pi}\exp\{j(B\sin u - ku)du \tag{25}$$

and thus

$$\begin{aligned} s_R(t) &= \rho\exp\left(j\frac{4\pi}{\lambda}R_0\right)\sum_{k=-\infty}^{\infty}J_k(B)\exp[j(2\pi f + k\omega_v)t] \\ &= \rho\exp\left(j\frac{4\pi}{\lambda}R_0\right) \\ &\quad\times\{J_0(B)\exp(j2\pi ft) \\ &\quad + J_1(B)\exp[j(2\pi f+\omega_v)t] \\ &\quad - J_1(B)\exp[j(2\pi f-\omega_v)t] \\ &\quad + J_2(B)\exp[j(2\pi f+2\omega_v)t] \\ &\quad + J_2(B)\exp[j(2\pi f-2\omega_v)t] \\ &\quad + J_3(B)\exp[j(2\pi f+3\omega_v)t] \\ &\quad - J_3(B)\exp[j(2\pi f-3\omega_v)t] + \cdots\}. \end{aligned} \tag{26}$$

Therefore, the micro-Doppler frequency spectrum consists of pairs of spectral lines around the center frequency f with spacing $\omega_v/(2\pi)$ between adjacent lines.

Because of the vibration, the point scatterer P, which initially at time $t = 0$ is located at $(X_0,Y_0,Z_0)^T$ in the (X,Y,Z) coordinates, will, at time t, move to

$$\begin{bmatrix} X \\ Y \\ Z \end{bmatrix} = D_v\sin(2\pi f_v t)\begin{bmatrix} \cos\alpha_P\cos\beta_P \\ \sin\alpha_P\cos\beta_P \\ \sin\beta_P \end{bmatrix} + \begin{bmatrix} X_0 \\ Y_0 \\ Z_0 \end{bmatrix}. \tag{27}$$

The velocity of the scatterer P due to the vibration becomes

$$\vec{v} = 2\pi D_v f_v\cos(2\pi f_v t)(\cos\alpha_P\cos\beta_P, \sin\alpha_P\cos\beta_P, \sin\beta_P)^T. \tag{28}$$

Based on (16), the micro-Doppler shift induced by the vibration is

$$\begin{aligned} f_{\text{micro-Doppler}} &= \frac{2f}{c}(\vec{v}^T\cdot\vec{n}) \\ &= \frac{4\pi f f_v D_v}{c}[\cos(\alpha-\alpha_P)\cos\beta\cos\beta_P \\ &\qquad + \sin\beta\sin\beta_P]\cos(2\pi f_v t). \end{aligned} \tag{29}$$

If the azimuth angle α and the elevation angle β_P are both zero, one has

$$f_{\text{micro-Doppler}} = \frac{4\pi f f_v D_v}{c}\cos\alpha_P\cos\beta\cos(2\pi f_v t). \tag{30}$$

When the orientation of the vibrating scatterer is along the projection of the radar LOS direction, or $\alpha_P = 0$, and the elevation angle β is also 0, the Doppler frequency change reaches the maximum value of $4\pi f f_v D_v/c$.

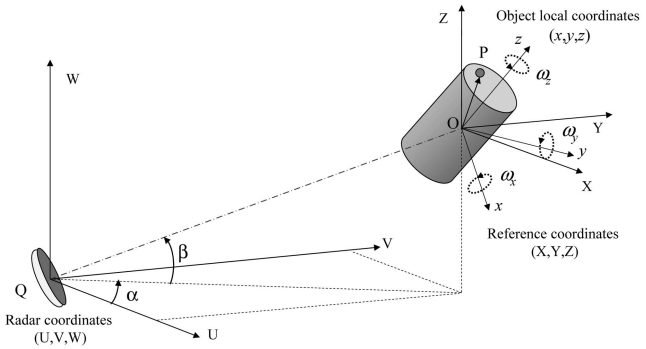

Fig. 4. Geometry of radar and rotating target.

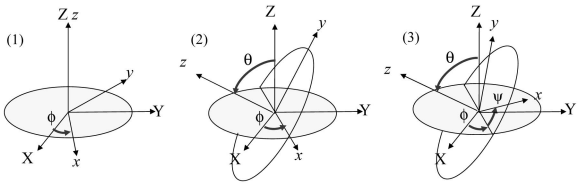

Fig. 5. Rotations by Euler angles (ϕ,θ,ψ).

B. Rotation-Induced Micro-Doppler Modulation

The geometry of a radar and a target with 3-dimensional rotations is illustrated in Fig. 4. The radar coordinate system is (U,V,W), the target local coordinate system is (x,y,z), and the reference coordinate system (X,Y,Z) is parallel to the radar coordinates (U,V,W) and located at the origin of the target local coordinates. Assume that the azimuth and elevation angle of the target in the radar coordinates (U,V,W) are α and β, respectively, and the unit vector of the radar LOS is the same as (18).

Due to the target's rotation, any point on the target described in the local coordinate system (x,y,z) will move to a new position in the reference coordinate system (X,Y,Z). The new position can be calculated from its initial position vector multiplied by an initial rotation matrix determined by Euler angles (ϕ,θ,ψ), where the angle ϕ rotates about the z-axis, the angle θ rotates about the x-axis, and the angle ψ rotates about the z-axis again, as illustrated in Fig. 5.

The corresponding initial rotation matrix is defined by

$$\begin{aligned}\Re_{\text{Init}} &= \begin{bmatrix} a_{11} & a_{12} & a_{13} \\ a_{21} & a_{22} & a_{23} \\ a_{31} & a_{32} & a_{33} \end{bmatrix} \\ &= \begin{bmatrix} \cos\phi & -\sin\phi & 0 \\ \sin\phi & \cos\phi & 0 \\ 0 & 0 & 1 \end{bmatrix} \begin{bmatrix} 1 & 0 & 0 \\ 0 & \cos\theta & -\sin\theta \\ 0 & \sin\theta & \cos\theta \end{bmatrix} \\ &\quad \times \begin{bmatrix} \cos\psi & -\sin\psi & 0 \\ \sin\psi & \cos\psi & 0 \\ 0 & 0 & 1 \end{bmatrix} \end{aligned} \tag{31}$$

where

$$\begin{aligned} a_{11} &= \cos\phi\cos\psi - \sin\phi\cos\theta\sin\psi \\ a_{12} &= -\cos\phi\sin\psi - \sin\phi\cos\theta\cos\psi \\ a_{13} &= \sin\phi\sin\theta \\ a_{21} &= \sin\phi\cos\psi + \cos\phi\cos\theta\sin\psi \\ a_{22} &= -\sin\phi\sin\psi + \cos\phi\cos\theta\cos\psi \\ a_{23} &= -\cos\phi\sin\theta \\ a_{31} &= \sin\theta\sin\psi \\ a_{32} &= \sin\theta\cos\psi \\ a_{33} &= \cos\theta. \end{aligned}$$

Viewed in the target local coordinate system, when a target rotates about its axes x, y, and z with an angular velocity $\vec{\omega} = (\omega_x,\omega_y,\omega_z)^T$, a point scatterer P at $\vec{r}_0 = (x_0,y_0,z_0)^T$ represented in the target local coordinates (x,y,z) will move to a new location in the reference coordinate system described by $\Re_{\text{Init}} \cdot \vec{r}_0$ and the unit vector of the rotation becomes

$$\vec{\omega}' = (\omega'_x,\omega'_y,\omega'_z)^T = \frac{\Re_{\text{Init}} \cdot \vec{\omega}}{\|\vec{\omega}\|} \tag{32}$$

with the scalar angular velocity $\Omega = \|\vec{\omega}\|$. Thus, according to Rodrigues formula (see the Appendix) [15], at time t the rotation matrix becomes

$$\Re_t = I + \hat{\omega}' \sin\Omega t + \hat{\omega}'^2(1-\cos\Omega t) \tag{33}$$

where $\hat{\omega}'$ is a skew symmetric matrix

$$\hat{\omega}' = \begin{bmatrix} 0 & -\omega'_z & \omega'_y \\ \omega'_z & 0 & -\omega'_x \\ -\omega'_y & \omega'_x & 0 \end{bmatrix}. \tag{34}$$

Viewed in the reference coordinate system (X,Y,Z), at time t, the scatterer P will move from its initial location to a new location $\vec{r} = \Re_t \cdot \Re_{\text{Init}} \cdot \vec{r}_0$. According to (17), the micro-Doppler frequency shift induced by the rotation is approximately

$$\begin{aligned} f_{\text{micro-Doppler}} &= \frac{2f}{c}[\Omega\vec{\omega}' \times \vec{r}]_{\text{radial}} = \frac{2f}{c}(\Omega\hat{\omega}'\vec{r})^T \cdot \vec{n} \\ &= \frac{2f}{c}[\Omega\hat{\omega}'\Re_t \cdot \Re_{\text{Init}} \cdot \vec{r}_0]^T \cdot \vec{n} \\ &= \frac{2f\Omega}{c}\{[\hat{\omega}'^2 \sin\Omega t - \hat{\omega}'^3\cos\Omega t \\ &\qquad + \hat{\omega}'(I+\hat{\omega}'^2)]\Re_{\text{Init}} \cdot \vec{r}_0\}^T \cdot \vec{n}. \end{aligned} \tag{35}$$

If the skew symmetric matrix $\hat{\omega}'$ is defined by a unit vector, then $\hat{\omega}'^3 = -\hat{\omega}'$ and the rotation-induced

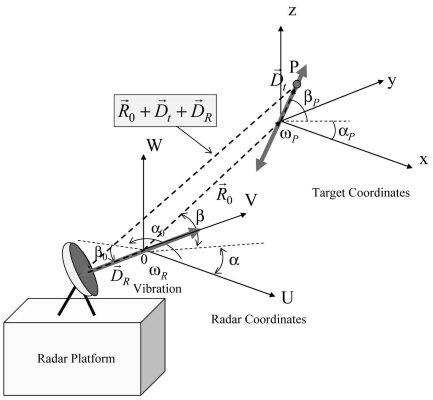

Fig. 6. Geometry of radar platform vibration.

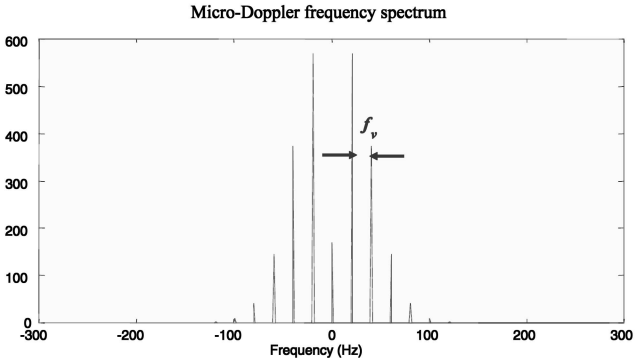

Fig. 7. Frequency representation of signal reflected from vibrating scatterer.

micro-Doppler frequency becomes

$$f_{\text{micro-Doppler}} = \frac{2f\Omega}{c}[\hat{\omega}'(\hat{\omega}'\sin\Omega t + I\cos\Omega t)\Re_{\text{Init}}\cdot\vec{r}_0]_{\text{radial}}. \tag{36}$$

C. Effect of Radar Platform Vibration on Micro-Doppler Modulation

If the radar platform is also vibrating, the radar can be moved from the origin of the coordinate system (U,V,W) at a distance D_R as shown in Fig. 6. Thus, the vector from the radar to a scatterer P on the target becomes $\vec{R}_t = \vec{R}_0 + \vec{D}_t - \vec{D}_R$ where $\vec{D}_R$ represents the component of the platform's vibration. Thus, if the azimuth angle α of the center point O is zero, the range from the radar to the scatterer P becomes

$$\begin{aligned} R(t) = R_0 &+ D_v\sin\omega_v t\cdot(\cos\alpha_P\cos\beta_P\cos\beta + \sin\beta_P\sin\beta) \\ &- D_R\sin\omega_R t\cdot(\cos\alpha_0\cos\beta_0\cos\beta + \sin\beta_0\sin\beta) \end{aligned} \tag{37}$$

where ω_R is the platform vibration rate in angular frequency, D_R is the amplitude of the platform vibration, and α_0 and β_0 are the azimuth and elevation angles of the direction of radar platform vibration with respect to the initial radar origin point.

If the platform vibration and the target vibration are in the same direction ($\alpha_0 = \alpha_P$ and $\beta_0 = \beta_P$), the vibration of the radar platform is superimposed onto the target's vibration. Otherwise, the platform vibration may have a more complex effect on the micro-Doppler modulation.

The micro-Doppler modulation induced by these vibrations becomes

$$\begin{aligned} &f_{\text{micro-Doppler}} \\ &= \frac{1}{2\pi}\frac{d\Phi}{dt} = \frac{2}{\lambda}\frac{dR(t)}{dt} \\ &= \frac{2}{\lambda}D_v\omega_v[\cos(\alpha-\alpha_p)\cos\beta\cos\beta_p + \sin\beta\sin\beta_p]\cos\omega_v t \\ &\quad - \frac{2}{\lambda}D_R\omega_R[\cos(\alpha-\alpha_0)\cos\beta_0\cos\beta + \sin\beta_0\sin\beta]\cos\omega_R t. \end{aligned} \tag{38}$$

The second term is the micro-Doppler variation caused by the platform vibration. When $\alpha = \alpha_P = \alpha_0$ and $\beta = \beta_P = \beta_0 = 0$, the micro-Doppler modulation becomes

$$\Delta f_{\text{micro-Doppler}} = \frac{2}{\lambda}(D_v\omega_v\cos\omega_v t - D_R\omega_R\cos\omega_R t). \tag{39}$$

If the radar platform vibrates at a lower rate, for eliminating the variation caused by the platform vibration, a low-pass filter may be used to extract and remove the second micro-Doppler modulation term. The platform vibration can also be filtered out in the joint time-frequency domain by applying a time-frequency filtering.

III. TIME-FREQUENCY ANALYSIS OF MICRO-DOPPLER MODULATION

The Fourier transform is the most common method to analyze the properties of a signal waveform in the frequency domain. It shows the distribution of the magnitude and the phase at different frequencies contained in the signal during the time interval of analyzing. When a signal is reflected from a rotating target, the frequency spectrum of the signal may indicate the presence of micro-Doppler modulation. Micro-Doppler effect can be observed by deviations of the frequency spectrum from the center frequency. Fig. 7 shows the frequency spectrum of a signal reflected by a vibrating point scatterer. The micro-Doppler frequencies are centered at 0 with an equal displacement toward each side, suggesting that the point scatterer could have been vibrating along the radar LOS with equal magnitude toward each direction.

Due to lack of localized time information, the Fourier transform, however, cannot provide more complicated time-varying frequency modulation information. A joint time-frequency analysis that provides localized time-dependent frequency information is needed for extracting time-varying motion dynamic features.

TABLE I
Bilinear Time-Frequency Transforms

TF Transforms	Formula	Kernel
Cohen Class	$C(t,\omega)=\iiint \Phi(\theta,\tau)s\left(u+\frac{\tau}{2}\right)s^*\left(u+\frac{\tau}{2}\right)e^{-j\theta t-j\omega\tau+j\theta u}du\,d\tau\,d\theta$	$\Phi(\theta,\tau)$
Wigner-Ville	$\mathrm{WVD}(t,\omega)=\int s\left(t+\frac{\tau}{2}\right)s^*\left(t+\frac{\tau}{2}\right)\exp\{-j\omega\tau\}d\tau$	$\Phi(\theta,\tau)=1$
Choi-Williams	$CW(t,\omega,\sigma)=\iint K_{CW}(u-t,\tau)s\left(u+\frac{\tau}{2}\right)s^*\left(u+\frac{\tau}{2}\right)e^{-j\omega\tau}du\,d\tau$	$\Phi(\theta,\tau)=K_{CW}(\theta,\tau)=\frac{1}{4\pi^{3/2}\sqrt{\tau^2/\sigma}}\exp\{-\theta^2\tau^2/\sigma\}$
Pseudo Wigner	$PWD(t,\omega,\alpha)=\int h(\tau)s\left(t+\frac{\tau}{2}\right)s^*\left(t+\frac{\tau}{2}\right)\exp\{-j\omega\tau\}d\tau$	$\Phi(\theta,\tau)=h(\tau)=\exp\{j\alpha\tau^2/2\}$
Smooth Pseudo Wigner-Ville (SPWV)	$SPWD(t,\omega,\alpha)=\int s(t-u)PWD(t,\omega,\alpha)du$	$\Phi(\theta,\tau)=h(\tau)=\exp\{j\alpha\tau^2/2\}$
Cone Kernel	$CKD(t,\omega)=\iiint K_{CK}(t-u,\tau)s\left(u+\frac{\tau}{2}\right)s^*\left(u+\frac{\tau}{2}\right)e^{-j\omega\tau}du\,d\tau$	$\Phi(\theta,\tau)=K_{CK}(t,\tau)=\begin{cases}g(\tau); & \lvert t/\tau\rvert<1/2\\ 0; & \lvert t/\tau\rvert>1/2\end{cases}$

To analyze the time-varying frequency characteristics of the micro-Doppler modulation and visualize the localized joint time and frequency information, the signal must be analyzed by using a high-resolution time-frequency transform, which characterizes the temporal and spectral behavior of the analyzed signal. For example, by examining the time information and the sign of the micro-Doppler shift caused by a movement, the direction of the movement at the specific time could be found.

Time-frequency transforms includes linear transforms, such as the short-time Fourier transform (STFT), and bilinear transforms, such as the Wigner-Ville distribution (WVD). With a time-limited window function, the resolution of the STFT is determined by the window size. There is a trade-off between the time resolution and the frequency resolution. A larger window has higher frequency resolution but a poorer time resolution. The well-known spectrogram defined as the square modulus of the STFT is a popular tool for time-frequency analysis.

The WVD of a signal $s(t)$ is defined as the Fourier transform of the time-dependent autocorrelation function

$$\mathrm{WVD}(t,\omega)=\int s\left(t+\frac{t'}{2}\right)s^*\left(t-\frac{t'}{2}\right)\exp\{-j\omega t'\}dt' \tag{40}$$

where $s(t+(t'/2))s^*(t-(t'/2))$ can be seen as a time-dependent autocorrelation function. The bilinear WVD has better joint time-frequency resolution than any linear transform. It suffers, however, from a problem of cross-term interference, i.e., the WVD of the sum of two signals is not the sum of their individual WVDs. If a signal contains more than one component in the joint time-frequency domain, its WVD will contain cross terms that occur halfway between each pair of auto-terms. The magnitude of these oscillatory cross terms can be twice as large as the auto-terms.

To reduce the cross-term interference, the filtered WVD has been used to preserve the useful properties of the time-frequency transform with a slightly reduced time-frequency resolution and largely reduced cross-term interference. The WVD with a linear low-pass filter belongs to Cohen's class [18, 19].

The general form of Cohen's class is defined as

$$C(t,\omega)=\iint s\left(u+\frac{\tau}{2}\right)s^*\left(u-\frac{\tau}{2}\right)\times\phi(t-u,\tau)\exp\{-j\omega\tau\}du\,d\tau. \tag{41}$$

The Fourier transform of $\phi(t,\tau)$, denoted as $\Phi(\theta,\tau)$, is called the kernel function. It can easily be seen that if $\Phi(\theta,\tau)=1$, then $\phi(t,\tau)=\delta(t)$ and the Cohen class reduces to the WVD. Other types of kernel functions, which lead to the Choi-Williams distribution, the pseudo Wigner, the smoothed pseudo Wigner-Ville and the cone kernel distribution (see Table I), can be designed to reduce the cross-term interference problem of the WVD.

Other high-resolution time-frequency transform includes the adaptive time-frequency transform [18]. It decomposes a signal into a family of basis functions, such as the Gabor function (a Gaussian modulated exponential function), which is well localized in both the time and the frequency domain and adaptive to match the local behavior of the analyzed signal. The adaptive Gaussian representation is a signal-adaptive, high-resolution transform. It expands a signal $s(t)$ in terms of Gabor basis functions $h_p(t)$ with an adjustable standard deviation s_p and a time-frequency center (t_p,f_p):

$$s(t)=\sum_{p=1}^{\infty}B_p h_p(t) \tag{42}$$

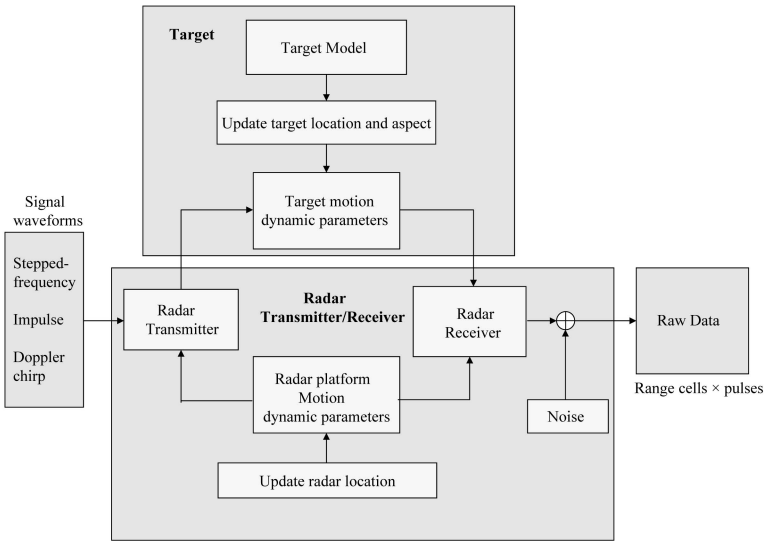

Fig. 8. Block diagram of simulation.

where

$$h_p(t) = (\pi\sigma_p^2)^{-0.25} \exp\left[-\frac{(t-t_p)^2}{2\sigma_p^2}\right] \exp(j2\pi f_p t). \tag{43}$$

The coefficients B_p are found by an iterative procedure beginning with the stage $p = 1$ and choosing the parameters σ_p, t_p, and f_p such that $h_p(t)$ is most similar to $s(t)$:

$$|B_p|^2 = \max_{\sigma_p, t_p, f_p} \left| \int s_{p-1}(t) h_p^*(t) dt \right|^2 \tag{44}$$

where $s_0(t) = s(t)$, i.e., the analyzed signal is taken as the initial signal for $p = 1$. For $p > 1$, $s_p(t)$ is the residual after the orthogonal projection of $s_{p-1}(t)$ onto $h_p(t)$ has been removed from the signal:

$$s_p(t) = s_{p-1}(t) - B_p(t) h_p(t). \tag{45}$$

This procedure is iterated to generate as many coefficients as needed to accurately represent the original signal.

In principle, any time-frequency transform can be used to analyze micro-Doppler modulations. However, a desired time-frequency transform should satisfy the requirements on high resolution in both the time and frequency domains and low cross-term interference. The smoothed pseudo Wigner-Ville distribution in Table I is a good candidate for analyzing micro-Doppler modulations due to its slightly reduced time-frequency resolution and largely reduced cross-term interference. The adaptive time-frequency transform is also a good candidate and has advantages over conventional time-frequency techniques (such as STFT). It is a parametric procedure that not only results in very high time-frequency resolution but also allows to separate different target's features (such as the swinging arm feature and the body motion feature of a walking man) using their different components along the basis functions.

IV. SIMULATION STUDY OF MICRO-DOPPLER MODULATIONS INDUCED BY MICRO-MOTION DYNAMICS

In this section, we present several examples of micro-motions that can induce micro-Doppler modulations. Based on the basic model described in Section II, several useful formulas of micro-Doppler modulations are derived. We compare the theoretical results with those generated by computer simulation. In the simulation, the target is defined in terms of a 3D reflectivity density function characterized by point scatterers. No occlusion effect is considered in target models. We select the point scatterer model in the simulation study because of its simplicity compared with electromagnetic prediction codes (such as the Xpatch), its ability to incorporate any target's motion into the simulation, and its capability to investigate the effect of individual motion components. In both the simulated micro-Doppler modulations and the theoretical micro-Doppler modulations calculated from the corresponding formulas, we use the same target model with the same micro motions. The simulation, however, does not presuppose any theoretical formulas of micro-Doppler modulations. It is based on physical properties of electromagnetic backscattering from a rigid body undergoing nonlinear dynamics. The purpose of the simulation is to verify the theoretical results. The comparison shows that the simulation result and the theoretical result are identical, and thus verifies the theoretical formulation of micro-Doppler modulations.

Fig. 8 is the block diagram of the simulation. The system mainly consists of three parts: the radar transmitted signal, the target, and the radar received

signal. The transmitted signal can be a step-frequency waveform, an impulse waveform, a Doppler chirp waveform, or other defined waveforms. The target is given by a set of point scatterers described by their reflectivity and locations in the target local coordinate system (x,y,z) embedded on the target, their origin at the geometric center while the x-axis is defined as the heading direction of the target. The radar is located at the origin of the radar coordinates (U,V,W). Both the radar and the target coordinates can have translations and rotations with respect to the Earth center Earth fixed (ECEF) system. Initial locations, velocities, accelerations and trajectories of the radar and the target coordinates are predetermined as inputs to the simulation.

Based on the returned signal from a single point scatterer, the returned signal from the target can be represented as the summation of the returned signals from all scatterer centers in the target. For a given PRF, the transmitter repeatedly transmits signals. For each transmitted signal, the returned signal from the target must be updated according to the updated range for each point scatterer on the target due to its translation and rotations. Then, the returned signals can be rearranged into a two-dimensional (the number of range cells by the number of pulses) data matrix, which is the raw data to be analyzed. In summary, the simulation procedure includes [19]:

1) select radar parameters (the carrier frequency, bandwidth, signal waveform, and PRF);
2) select radar motion parameters (the initial location, trajectory, velocity, and acceleration in the ECEF system);
3) select predesigned point scatterer model of the target;
4) select target motion parameters (the initial location, trajectory, velocity, and acceleration in the ECEF system);
5) transmit signal pulse repeatedly to the target, update the radar and the target locations, and calculate received signals;
6) select signal-to-noise ratio (SNR) for the raw data and add the calculated noise level to the raw data;
7) arrange the received raw data into a 2-dimensional (range $\times$ pulse) matrix.

In the simulation procedure, no mathematical formula on micro-Doppler modulations is implemented.

A. Vibrating Target

Vibration is a basic micro-motion of a target. Examples of vibrations include engine-induced surface vibration and mechanical oscillations of a bridge or a building. The geometry of the radar and a vibrating point scatterer is shown in Fig. 9(a). The vibration center O is stationary with azimuth angle α and elevation angle β with respect to the radar. The scatterer is vibrating at a vibration frequency f_v and amplitude D_v. The azimuth and elevation angle of the vibrating direction are α_P and β_P, respectively, described in the reference coordinates (X,Y,Z). Then, with the unit vector of the radar LOS given in (18), the point scatterer P, which is initially located at time $t = 0$ at (X_0,Y_0,Z_0) in (X,Y,Z), will move at time t to

$$\begin{bmatrix} X \\ Y \\ Z \end{bmatrix} = D_v \sin(2\pi f_v t) \begin{bmatrix} \cos\alpha_P \cos\beta_P \\ \sin\alpha_P \cos\beta_P \\ \sin\beta_P \end{bmatrix} + \begin{bmatrix} X_0 \\ Y_0 \\ Z_0 \end{bmatrix} \tag{46}$$

as indicated in (27). The micro-Doppler modulation induced by the vibration is derived in (29)

$$f_{\text{micro-Doppler}} = \frac{4\pi f f_v D_v}{c}[\cos(\alpha-\alpha_P)\cos\beta\cos\beta_P + \sin\beta\sin\beta_P]\cos(2\pi f_v t). \tag{47}$$

Assume the radar operates at 10 GHz and transmits a pulse waveform with a PRF of 2,000. Given $D_v = 0.01$ m, $f_v = 2$ Hz, $\alpha_P = 30°$, $\beta_P = 30°$, and the center of the vibration at ($U = 1000$ m, $V = 5000$ m, $W = 5000$ m), the theoretical result of the micro-Doppler modulation is shown in Fig. 9(b), while the simulation result shown in Fig. 9(c) is identical to the theoretical analysis.

B. Rotating Target

Rotation is another basic micro-motion of a target. Examples of rotations include rotor blades of a helicopter or a rotating antenna on a ship. The geometry of the radar and a 3-dimensional rotating target is depicted in Fig. 10(a). The radar coordinate system is defined by (U,V,W); the target local coordinate system is defined by (x,y,z); and the reference coordinate system (X,Y,Z) is parallel to the radar coordinates (U,V,W) and located at the origin of the target local coordinates. The azimuth and elevation angle of the target with respect to the radar coordinates (U,V,W) are α and β, respectively.

Assume the target rotates about its axes x, y, and z with an angular velocity vector $\vec{\omega} = (\omega_x,\omega_y,\omega_z)^T$ or a scalar angular velocity $\Omega = \|\vec{\omega}\|$. The corresponding initial rotation matrix $\Re_{\text{Init}}$ is given in (31). If a point scatterer P is initially located at $\vec{r}_0 = (x_0,y_0,z_0)^T$ in the local coordinates (x,y,z), then viewing from the reference coordinates system (X,Y,Z) the point scatterer P will move to $\Re_{\text{Init}} \cdot \vec{r}_0$ through rotating along the unit vector

$$\vec{\omega}' = (\omega'_x,\omega'_y,\omega'_z)^T$$

given in (32). Therefore, reviewing in the reference coordinate system (X,Y,Z), at time t the scatterer P

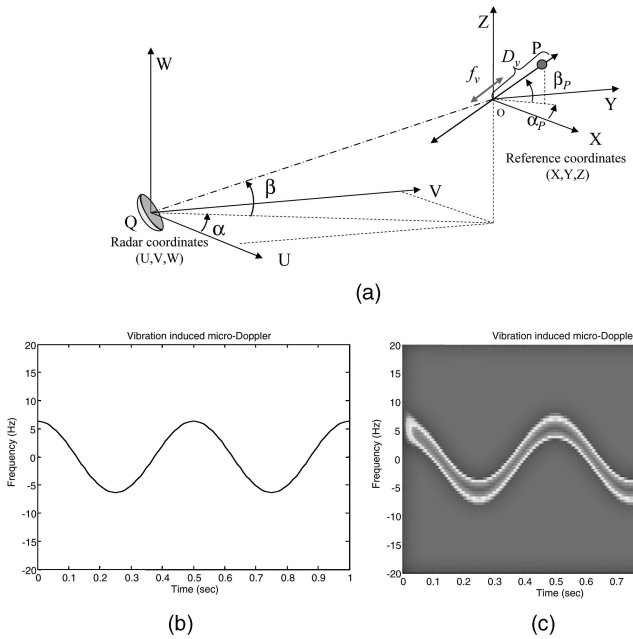

Fig. 9. Micro-Doppler modulation induced by vibration.

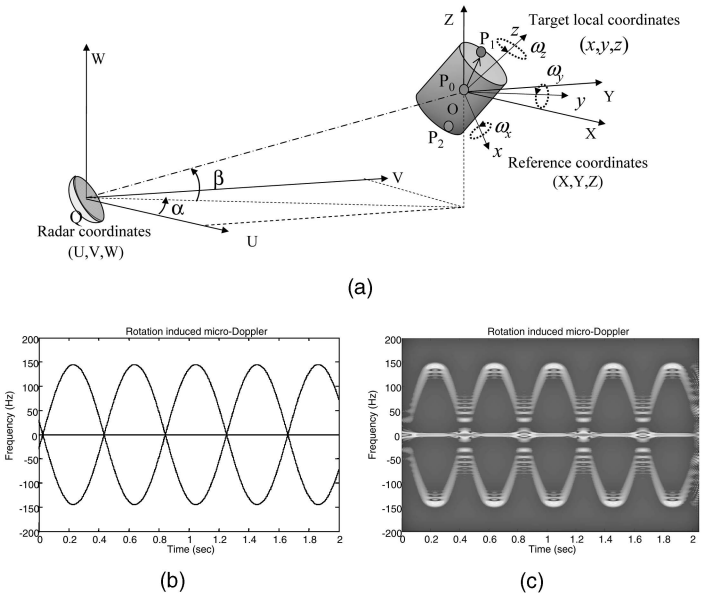

Fig. 10. Micro-Doppler modulation induced by rotation.

will move to $\vec{r} = \Re_t \cdot \Re_{\text{Init}} \cdot \vec{r}_0$. According to (35), if $\hat{\omega}'^3 = -\hat{\omega}'$, the micro-Doppler modulation of the point scatterer becomes

$$f_{\text{micro-Doppler}} = \frac{2f\Omega}{c}[\hat{\omega}'(\hat{\omega}' \sin\Omega t + I\cos\Omega t)\Re_{\text{Init}} \cdot \vec{r}_0]_{\text{radial}}$$

as given in (36), and the micro-Doppler signature in the time-frequency domain is a sinusoidal function of Ω with an initial phase and amplitude depending on the initial position and the initial Euler angles (ϕ, θ, ψ) of the point scatterer.

Assume that the radar operates at 10 GHz and a target, located at (U = 1000 m, V = 5000 m, W = 5000 m), is rotating along the x, y, and z axes with an initial Euler angles ($\phi = 30°$, $\theta = 20°$, $\psi = 20°$) and angular velocity $\vec{\omega} = [\pi, 2\pi, \pi]^T$ rad/s. Suppose the target has three strong scatterer centers: scatterer P_0 (the center of the rotation) is located at (x = 0 m, y = 0 m, z = 0 m); scatterer P_1 is located at (x = 1.0 m, y = 0.6 m, z = 0.8 m); and scatterer P_2 is located at (x = −1.0 m, y = −0.6 m, z = −0.8 m). The theoretical micro-Doppler modulation calculated by (36) is shown in Fig. 10(b). The micro-Doppler of the center point P_0 is the line at the zero frequency, and micro-Doppler modulations from the point P_1 and P_2 are the two sinusoidal curves about the zero frequency. Given a radar PRF of 1,000 pulse/s and 2,048 pulses transmitted during 2.05 s of dwell time,

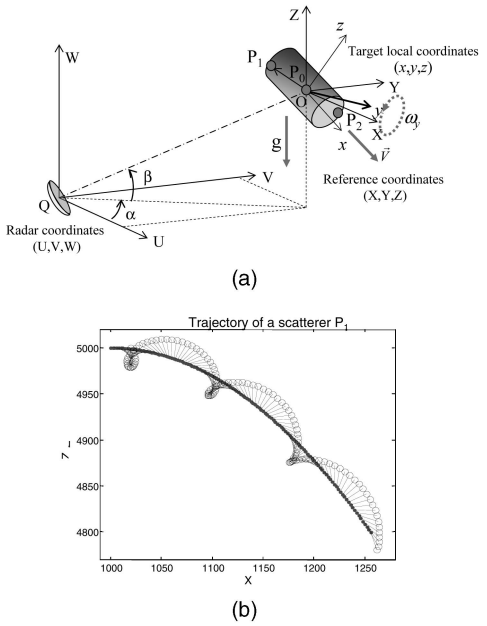

Fig. 11. (a) Geometry of radar and tumbling target. (b) Trajectory of scatterer in tumbling target.

the simulated micro-Doppler modulation signature is shown in the Fig. 10(c), which is identical to the theoretical analysis. The rotation period can be obtained from the rotation angular velocity as $T = 2\pi/\|\vec{\omega}\| = 0.8165$ s and is verified by both the theoretical result and the simulated result.

C. Tumbling Target

Tumbling is a rotation accompanied by translation and acceleration. Examples of target tumbling include a spacecraft tumbling through space or a fuel tank of a missile tumbling after its separation from the reentry vehicle. Tumbling target with translation, acceleration, and rotation is illustrated in Fig. 11(a). Assume the target has an initial translation velocity $\vec{V}$ along the x-axis and an acceleration of $g = 9.8$ m/s^2, due to gravity, with respect to the radar coordinates. At the same time, the target rotates along the y-axis with an angular velocity ω_y. The azimuth and elevation angle of the origin O of the target local coordinates with respect to the origin of the radar coordinates are α and β, respectively. The reference coordinate system (X,Y,Z), which is parallel to the radar coordinates (U,V,W) and shares the same origin O with the target local coordinates (x,y,z), has the same initial velocity and acceleration as the target but has no rotation with respect to the radar coordinates. Thus, the location of any point scatterer of the target in (X,Y,Z) can be calculated by multiplying the location of the scatterer in (x,y,z) with an initial rotation matrix $\Re_{\text{Init}}$ defined by the initial Euler angles (ϕ,θ,ψ) given in (31). Assuming the initial location of a scatterer P_1 is at $\vec{r}_0 = [x,y,z]^T$ in the local coordinate system, viewed from the reference coordinate system (X,Y,Z) the point scatterer P_1 will move to $\Re_{\text{Init}} \cdot \vec{r}_0$ and the initial velocity of the target will be $\vec{V} = V \cdot [a_{11}, a_{21}, a_{31}]^T$, where a_{11}, a_{21}, and a_{31} are defined in (31).

Suppose the target rotates along the y-axis with an angular velocity $\omega = \omega_y$ rad/s. The trajectories of the target center of mass O and the scatterer P_1 are plotted in Fig. 11(b), where the dot-line is the trajectory of the target's center and the circled-line is the trajectory of the scatterer P_1. During tumbling, the length of the segment OP_1 stays constant. Viewed from the reference coordinates (X,Y,Z), the angular velocity of the target is $\vec{\omega}' = \omega \cdot [a_{12}, a_{22}, a_{32}]^T$ and the location of the scatterer P_1 will move to

$$\vec{r} = \Re_{\text{Init}} \begin{bmatrix} \cos\omega t & 0 & \sin\omega t \\ 0 & 1 & 0 \\ -\sin\omega t & 0 & \cos\omega t \end{bmatrix} \vec{r}_0. \tag{48}$$

Thus, the velocity of the target at time t becomes $\vec{V} = [Va_{11}, Va_{21}, Va_{31} - gt]^T$. According to the mathematical formula in (16), the Doppler frequency induced by the tumbling becomes

$$\begin{aligned} f_D &= \frac{2f}{c}[\vec{V} + \vec{\omega}' \times \vec{r}]_{\text{radial}} \\ &= \frac{2f}{c}(-\sin\beta gt + t_1) \\ &\quad + \frac{2f\omega}{c}[(xt_2 + zt_3)\cos\omega t + (zt_2 - xt_3)\sin\omega t] \end{aligned} \tag{49}$$

where

$$\begin{aligned} t_1 &= V[(a_{11}\cos\alpha + a_{21}\sin\alpha)\cos\beta + a_{31}\sin\beta] \\ t_2 &= [(a_{22}a_{31} - a_{32}a_{21})\cos\alpha + (a_{32}a_{11} - a_{12}a_{31})\sin\alpha]\cos\beta \\ &\quad + (a_{12}a_{21} - a_{22}a_{11})\sin\beta \\ t_3 &= [(a_{22}a_{33} - a_{32}a_{23})\cos\alpha + (a_{32}a_{13} - a_{12}a_{33})\sin\alpha]\cos\beta \\ &\quad + (a_{12}a_{23} - a_{22}a_{13})\sin\beta. \end{aligned} \tag{50}$$

The Doppler frequency shift induced by the initial velocity is

$$f_{D_{\text{Trans}}} = \frac{2f}{c}t_1 \tag{51}$$

and the micro-Doppler modulation induced by the rotation is

$$\begin{aligned} f_{\text{micro-Doppler}} &= \frac{2f\omega}{c}[(xt_2 + zt_3)\cos\omega t + (zt_2 - xt_3)\sin\omega t] \\ &\quad - \frac{2f}{c}\sin\beta \cdot gt. \end{aligned} \tag{52}$$

We notice that the micro-Doppler modulation induced by tumbling has a similar format as the micro-Doppler of rotation except an additional linear time-varying term determined by the gravity acceleration.

Assume now that the radar operates at 10 GHz and a target located at ($U = 1000$ m, $V = 5000$ m, $W = 5000$ m) is rotating along the y-axis with an angular

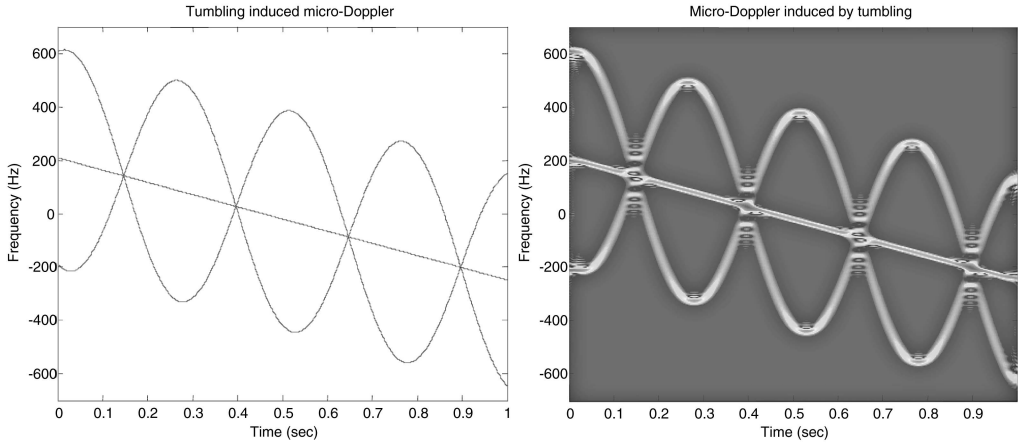

Fig. 12. Micro-Doppler modulations induced by target's tumbling.

velocity $\omega_y = 4\pi$ rad/s with initial Euler angles of $\phi = 20°$, $\theta = 20°$, $\psi = 20°$. If the initial velocity of the target is 5 m/s, the initial position of the scatterer P_0 is at the origin ($x = 0$ m, $y = 0$ m, $z = 0$ m), the scatterer P_1 is at ($x = -0.5$ m, $y = 0.3$ m, $z = 0.4$ m), and the scatterer P_2 is at ($x = 0.5$ m, $y = -0.3$ m, $z = -0.4$ m), then the theoretical micro-Doppler modulation is calculated by (52) and shown in Fig. 12(a). Due to gravity, the micro-Doppler of the point P_0 is a slope line starting at 200 Hz, and micro-Doppler modulations from the point P_1 and P_2 are the two sinusoidal curves around the slope line. For computer simulation, assuming the PRF is 3,000 pulse/s, i.e., 3,000 pulses can be transmitted within 1 s of dwell time, the simulated micro-Doppler modulation signature in the joint time-frequency domain is shown in Fig. 12(b), which is identical to the theoretical result. The rotation period can be obtained from the rotation angular velocity as $T = 2\pi/\|\vec{\omega}\| = 0.5$ s and is verified by both the theoretical result and the simulated result.

D. Coning Target

Coning motion is a rigid body rotation about an axis that intersects with an axis of the local coordinates. An example of the coning motion is the conning of a whipping top, which is a symmetric body spinning around its axis of symmetry and with one end point fixed. When its axis of symmetry is rotating about an axis that intersects with the axis of symmetry, the top is also doing coning motion. If the axis of symmetry does not remain at a constant angle with the axis of coning, it will oscillate up and down between two limits. This motion is called nutation. While a fuel tank of a missile is tumbling after its separation from the reentry vehicle as mentioned in Section IVC, the reentry vehicle will have spinning, coning, and nutation motions.

For simplicity, we only deal with target's coning motion without spinning and nutation. The geometry of the radar and a target with coning motion is depicted in Fig. 13(a). The radar is located at the origin of the radar coordinate system (U,V,W) and the target's local coordinate system is (x,y,z). The target has a coning motion along the axis $\overrightarrow{SN}$, which intersects with the z-axis at the point S ($x = 0$, $y = 0$, $z = z_0$) of the local coordinates. The reference coordinate system (X,Y,Z) is parallel to the radar coordinates (U,V,W) and its origin is located at the point S. Assume the azimuth and elevation angle of the target center O with respect to the radar are α and β, respectively, and the azimuth and elevation angle of the coning axis $\overrightarrow{SN}$ with respect to the reference coordinates (X,Y,Z) are α_N and β_N, respectively. Then, the unit vector of the radar LOS is

$$\vec{n} = [\cos\alpha\cos\beta, \sin\alpha\cos\beta, \sin\beta]^T$$

as given in (18), and the unit vector of the rotation axis in the reference coordinates (X,Y,Z) is

$$\vec{e} = [\cos\alpha_N\cos\beta_N, \sin\alpha_N\cos\beta_N, \sin\beta_N]^T. \quad (53)$$

Assume the initial position of a scatterer P_1 is $\vec{r}_0 = [x,y,z]^T$ represented in the target local coordinates. Then, the location of the point scatterer P_1 in the reference coordinates (X,Y,Z) can be calculated through its local coordinates by subtracting the coordinates of the point S and multiplying the rotation matrix $\Re_{\text{Init}}$ defined by the initial Euler angles (ϕ,θ,ψ). Viewed from the reference coordinates (X,Y,Z), the location of the scatterer P_1 is at $\Re_{\text{Init}} \cdot [x,y,z-z_0]^T$. Suppose the target has a coning motion with an angular velocity of ω rad/s. According to the Rodrigues's formula, at time t the rotation matrix in the (X,Y,Z) becomes

$$\Re_t = I + \hat{e}\sin\omega t + \hat{e}^2(1-\cos\omega t) \quad (54)$$

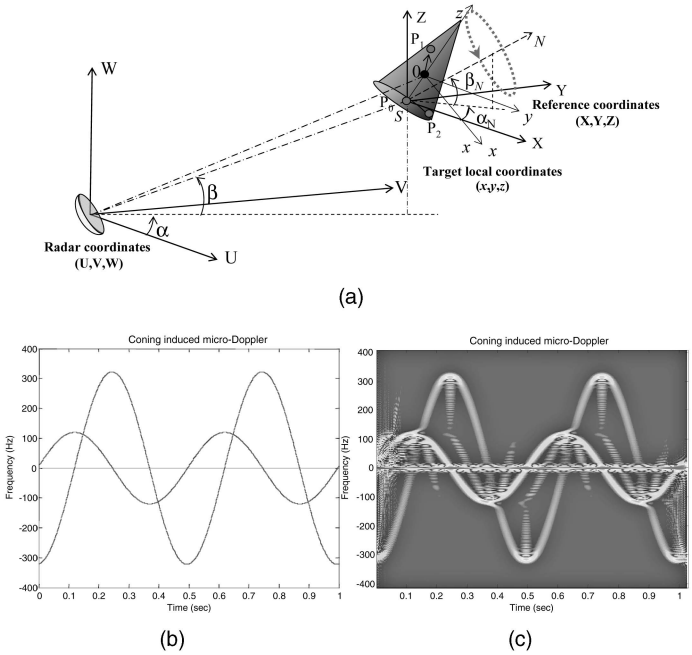

Fig. 13. (a) Geometry of radar and target with coning motion. (b) Calculated. (c) Simulated signatures of micro-Doppler modulation induced by coning motion.

where the skew symmetric matrix is defined by

$$\hat{e} = \begin{bmatrix} 0 & -\sin\beta_N & \sin\alpha_N\cos\beta_N \\ \sin\beta_N & 0 & -\cos\alpha_N\cos\beta_N \\ -\sin\alpha_N\cos\beta_N & \cos\alpha_N\cos\beta_N & 0 \end{bmatrix}. \tag{55}$$

Therefore, at time t the scatterer P_1 will move to $\vec{r}(t) = \Re_t \cdot \Re_{\text{Init}} \cdot [x, y, z - z_0]^T$.

If the point S is not too far from the target center of mass, we can approximate the radar LOS as the radial direction of the point S with respect to the radar. According to the mathematical formula (11) described in Section II, the micro-Doppler modulation induced by the coning motion is approximately

$$\begin{aligned} & f_{\text{micro-Doppler}} \\ &= \frac{2f}{c}\left[\frac{d}{dt}\vec{r}(t)\right]_{\text{radial}} = \frac{2f}{c}\left\{\left[\frac{d}{dt}\Re_t\right]\Re_{\text{Init}}\cdot[x,y,z-z_0]^T\right\}^T\cdot\vec{n} \\ &= \frac{2f\omega}{c}\{(\hat{e}\cos\omega t + \hat{e}^2\sin\omega t)\Re_{\text{Init}}\cdot[x,y,z-z_0]^T\}^T\cdot\vec{n}. \end{aligned} \tag{56}$$

Assume that the radar operates at 10 GHz and a target is initially located at (U = 1000 m, V = 5000 m, W = 5000 m). Suppose the initial Euler angles are $\phi = 30°$, $\theta = 30°$, and $\psi = 45°$, the target is coning with an angular velocity $\omega = 4\pi$ rad/s, and the azimuth and elevation angle of the rotation axis are $\alpha_N = 60°$ and $\beta_P = 45°$, respectively. Thus, given the location of the point S at (x = 0 m, y = 0 m, $z = -1$ m), the initial location of the scatterer P_0 at the point S, the scatterer P_1 at (x = 0.5 m, y = 0.6 m, z = 1.0 m), and the scatterer P_2 at ($x = -0.5$ m, $y = -0.6$ m, $z = -1.0$ m), then the theoretical micro-Doppler modulation calculated by (56) is shown in Fig. 13(b). The micro-Doppler of the point P_0 is zero frequency, and the micro-Doppler modulations from points P_1 and P_2 are the two sinusoidal curves about the zero frequency. For computer simulation, assuming the PRF is 2,000 pulse/s, i.e., 2,000 pulses can be transmitted within 1 s of dwell time, the simulated micro-Doppler modulation signature in the joint time-frequency domain is shown in Fig. 13(c), which is identical to the theoretical result and verifies that the rotation period is $T = 2\pi/\|\vec{\omega}\| = 0.5$ s.

V. APPLICATIONS OF MICRO-DOPPLER ANALYSIS

We have discussed the micro-Doppler effect in radar, joint time-frequency analysis of micro-Doppler modulations, and the simulation of micro-Doppler modulations using the point scattering model. In this section, we demonstrate the micro-Doppler effect in radar using measured real radar data and analyze micro-Doppler features embedded in radar signals using time-frequency analysis.

Radar signals returned from a rotating antenna on a ship, propellers of a fixed-wing aircraft, a rotor of a helicopter, or an engine compressor and blade assemblies of a jet aircraft, contain micro-Doppler characteristics related to the structures' rotation that can be used to determine the motion dynamics of these structures. Vibration generated by a vehicle engine can be detected by radar signals returned from the surface of the vehicle. Micro-Doppler signature of the engine vibration signal can be used to identify specific type of vehicles and determine

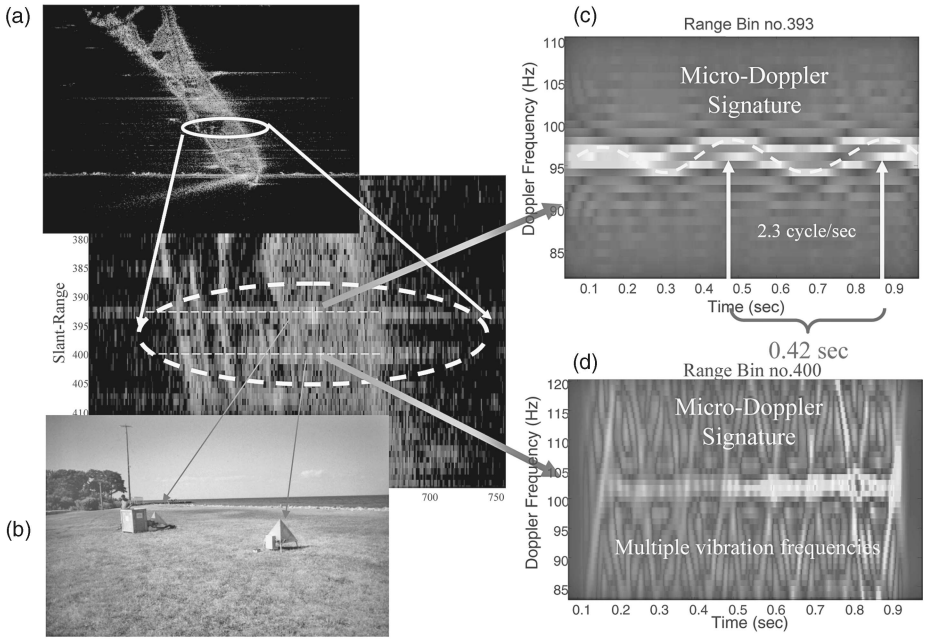

Fig. 14. Micro-Doppler signatures of vibrating cornel reflectors.

the movement and the speed of the engine. Natural mechanical oscillations of a bridge or a building can be also detected by the micro-Doppler modulations in radar returned signals. In Section VA, we analyze micro-Doppler signatures of two vibrating corner reflectors on the ground using measured real synthetic aperture radar data.

Human identification (ID) at a distance is the subject of increasing interest in biometrics and computer vision. Gait is a "gesture" of a walking person distinguishable from person to person. Gait analysis is a method of analyzing human motion from distance that offers a new way for human ID. A person will usually perform the same unique pattern when walking. It should be thus possible to recognize a person at a distance from their gait. Most efforts on human gait analysis are using image sequences. Here, in Section VB, we describe the micro-Doppler signature of a walking person using real radar data returned from the walking person.

A. Micro-Doppler Signature of Vibrating Corner Reflectors in SAR Scene

In synthetic aperture radar (SAR) image, oscillating targets may cause phase modulation on the azimuth phase history data. This phase modulation can be seen as a time-dependent micro-Doppler frequency shift. Based on micro-Doppler signatures in the time-frequency domain, references [20] and [21] calculated the oscillating frequency and amplitude of vibrating corner reflectors in a SAR scene.

Fig. 14(a) is a part of a SAR scene taken by X-band airborne SAR operating at 9.6 GHz with a PRF of 1,000 Hz. There are two corner reflectors on the ground as shown in Fig. 14(b). The reflectors were mechanically vibrating when the airborne SAR was illuminating the scene. As indicated in the zoomed area of Fig. 14(a), the two vibrating reflectors are located at range cell 393 and 400 in the SAR image. Due to vibration, SAR images of the two reflectors are smeared along the cross-range direction. In order to extract micro-Doppler signatures of the two vibrating reflectors, the phase history data, i.e., the raw data before forming a SAR image is used. By taking the phase history data at range cell 393 and suppressing the ground clutter returns, the micro-Doppler signature of the vibrating corner reflector can be seen in Fig. 14(c). It shows that the vibration rate of the corner reflector is 2.3 Hz, which is close to the ground truth of 2.0 Hz. In [21], the same data used in [20] is processed to calculate the amplitude of the vibration that turns out to be 1.5 mm. The micro-Doppler signature of the phase history data at range cell 400 shown in Fig. 15(d) indicates that the corner reflector at range cell 400 is vibrating at multiple vibration rates, which is coincident to the ground truth.

B. Micro-Doppler Signature of Human Walking Gait

Human walking is a complex motion that comprises different movements of individual body parts. The bulk motion of the body is basically a translation with slightly body rocking and head movement. The arms or legs swinging back and forth are strong micro-motions described by a partial rotation around an axis. Human experience shows that it is possible to recognize a friend by gait [22]. However, gait recognition by machine is a challenge.

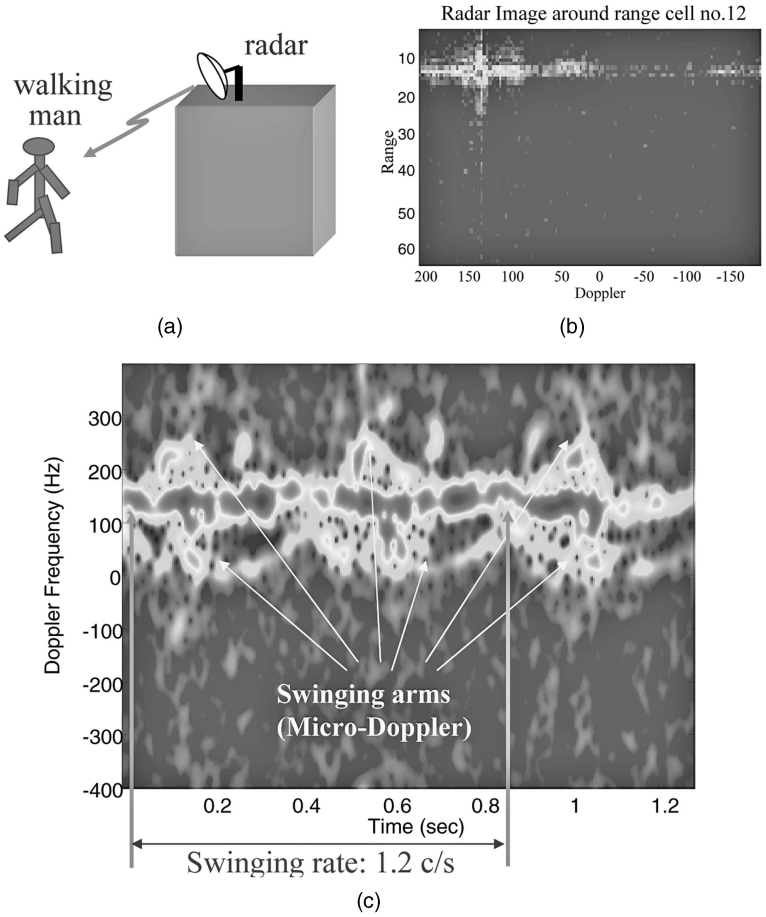

Fig. 15. Micro-Doppler signature of walking person with swinging arms.

Various computer vision and ultrasound techniques have been developed to measure gait parameters [23–28]. Radar gait analysis has recently been under development [29–32]. Radar has the advantage of detecting and identifying humans at distances in all weather conditions at day or night.

The micro-Doppler effect in radar returns from a walking person was studied in the late 1990s using data collected by a roof-top X-band high-resolution radar and reported in [29]. References [30] and [31] also studied the potential of using radar for gait analysis, where a fully coherent X-band CW radar was used to record signatures of human gait that contain rich information on the various parts of the moving body for human gait recognition. They simulated and analyzed gait cycle formed by the movements of various individual body parts. The gait signature was analyzed by the STFT. From the time-frequency signature of the human gait, each forward leg-swing can be seen by large peaks, and the left and right leg-swing completes a gait cycle. The body motion that is the stronger component underneath the leg-swings tends to have a slightly saw-tooth shape because the body speeds up and slows down during the swing. From the signature of a single gait cycle, the lower leg "eye hook" feature above the main body's Doppler frequency shift can be seen.

Recently, [32] reported the current progress on micro-Doppler analysis of human gait using radar. A human walking model and the detailed movement information on individual parts of a human body were proposed.

The measured radar data used in this paper was collected by a roof-top X-band radar (data provided by Norden Systems, Northrop Grumman). A man was walking towards the building at a speed of about 1.8 m/s as illustrated in Fig. 15(a). The range profile has 64 range cells and 1024 pulses were collected at a PRF of 800 Hz. Fig. 15(b) shows a radar range-Doppler image of the walking man using 64 range-cells and 128 pulses, where the hot spot in the image indicates the body of the walking man. One also notices a smeared line running across the Doppler direction around the body of the walking man at range cell 12.

By applying the STFT to the complex phase history data at range cell 12, the body Doppler shift and the micro-Doppler modulation of the swinging arms can be clearly detected in the joint time-frequency signature. The Doppler shift of one arm is higher and the other is lower than the

body Doppler frequency shift. Superposition of the time-frequency signatures over all range cells, which corresponds to different walking steps, gives a full time-frequency signature of the walking man as shown in Fig. 15(c). We can see that the body's Doppler shift is almost constant with a slightly saw-tooth shape but the arm's micro-Doppler shift is a time-varying periodic curve. From the available time information, the swinging rate of the arm can be estimated to about 1.2 cycle/s.

VI. SUMMARY

This paper introduced the micro-Doppler phenomenon in radar, derived mathematical formulas solving micro-Doppler modulations induced by vibration, rotation, tumbling, and coning motions, and applied point scatterer target's model to micro-Doppler simulation studies. By comparing the theoretical results with simulation results, we confirmed the effectiveness of our theoretical results. We also described applications of micro-Doppler analysis in radar and demonstrated examples of the micro-Doppler effect using real radar data. From the extracted micro-Doppler signatures, information about target's micro-motion dynamics, such as vibration rate of the cornel reflector and swinging rate of arms, can be obtained.

The usage of time-frequency analysis for extracting micro-Doppler signatures in clutter and noise environment, and applications of micro-Doppler analysis in radar to biometric identification, engine diagnosis, and detection of propeller modulations using an experimental X-band micro-Doppler radar will be reported in a separate paper in the near future.

APPENDIX

For any vector $\vec{u} = [u_x, u_y, u_z]^T$ and $\vec{r}$, define a skew symmetric matrix

$$\hat{u} = \begin{bmatrix} 0 & -u_z & u_y \\ u_z & 0 & -u_x \\ -u_y & u_x & 0 \end{bmatrix}. \tag{57}$$

The cross product of two vectors can be computed through matrix computation, that is,

$$\vec{p} = \vec{u} \times \vec{r} = \begin{bmatrix} u_y r_z - u_z r_y \\ u_z r_x - u_x r_z \\ u_x r_y - u_y r_x \end{bmatrix} = \begin{bmatrix} 0 & -u_z & u_y \\ u_z & 0 & -u_x \\ -u_y & u_x & 0 \end{bmatrix} \begin{bmatrix} r_x \\ r_y \\ r_z \end{bmatrix} = \hat{u}\vec{r}. \tag{58}$$

This definition is very useful in analysis of SO(3) groups (special orthogonal matrix groups, also called 3D rotation matrix), which are defined by:

$$\mathrm{SO}(3) = \{R \in \Re^{3\times 3} \mid R^T R = I, \det(R) = +1\}. \tag{59}$$

Computing the derivative of the constraint $R(t)R^T(t) = I$ with respect to time t, we obtain

$$\dot{R}(t)R^T(t) + R(t)\dot{R}^T(t) = 0 \quad \Rightarrow \quad \dot{R}(t)R^T(t) = -[\dot{R}(t)R^T(t)]^T.$$

The result reflects the fact that the matrix $\dot{R}(t)R^T(t) \in \Re^{3\times 3}$ is a skew symmetric matrix. Then there must exist a vector $\vec{\omega} \in \Re^3$ such that:

$$\hat{\omega} = \dot{R}(t)R^T(t). \tag{60}$$

Multiplying both sides by $R(t)$ to the right yields:

$$\dot{R}(t) = \hat{\omega}R(t). \tag{61}$$

Assume that the vector $\vec{\omega} \in \Re^3$ is constant. According to the linear ordinary differential equation (ODE), we can obtain:

$$R(t) = \exp\{\hat{\omega}t\}R(0) \tag{62}$$

where $\exp\{\hat{\omega}t\}$is the matrix exponential:

$$\exp\{\hat{\omega}t\} = I + \hat{\omega}t + \frac{(\hat{\omega}t)^2}{2!} + \cdots + \frac{(\hat{\omega}t)^n}{n!} + \cdots. \tag{63}$$

Assuming $R(0) = I$ for the initial condition we must have

$$R(t) = \exp\{\hat{\omega}t\}. \tag{64}$$

One can conform that the matrix $\exp\{\hat{\omega}t\}$ is indeed a rotation matrix. Since

$$[\exp(\omega t)]^{-1} = \exp(-\hat{\omega}t) = \exp(\hat{\omega}^T t) = [\exp(-\hat{\omega}t)]^T \tag{65}$$

then $[\exp(\hat{\omega}t)]^T(\exp(\hat{\omega}t)) = I$, from which one can obtain $\det[\exp(\hat{\omega}t)] = \pm 1$. Furthermore,

$$\det[\exp(\hat{\omega}t)] = \det\left[\exp\left(\frac{\hat{\omega}t}{2}\right) \cdot \exp\left(\frac{\hat{\omega}t}{2}\right)\right] = \left\{\det\left[\exp\left(\frac{\hat{\omega}t}{2}\right)\right]\right\}^2 \geq 0$$

which shows that $\det[\exp(\hat{\omega}t)] = +1$. Therefore, matrix $R(t) = \exp\{\hat{\omega}t\}$ is the 3D rotation matrix. Let $\Omega = \|\vec{\omega}\|$. A physical interpretation of the equation $R(t) = \exp\{\hat{\omega}t\}$ is simply a rotation around the axis $\vec{\omega} \in \Re^3$ by Ωt rad. If the rotation axis and the scalar angular velocity are given by vector $\vec{\omega} \in \Re^3$, the rotation matrix can be computed as $R(t) = \exp\{\hat{\omega}t\}$ at time t.

Rodrigues's formula is one efficient way to compute the rotation matrix $R(t) = \exp\{\hat{\omega}t\}$. Given $\vec{\omega}' \in \Re^3$ with $\|\vec{\omega}'\| = 1$ and $\vec{\omega} = \Omega\vec{\omega}'$, it is simple to verify that the power of $\hat{\omega}'$ can be reduced by the following formula:

$$\hat{\omega}'^3 = -\hat{\omega}'. \tag{66}$$

Then the exponential series

$$\exp(\hat{\omega}t) = I + \hat{\omega}t + \frac{(\hat{\omega}t)^2}{2!} + \cdots + \frac{(\hat{\omega}t)^n}{n!} + \cdots \quad (67)$$

can be simplified as

$$\begin{aligned}\exp(\hat{\omega}t) &= I + \left(\Omega t - \frac{(\Omega t)^3}{3!} + \frac{(\Omega t)^5}{5!} - \cdots\right)\hat{\omega}' \\ &\quad + \left(\frac{(\Omega t)^2}{2!} - \frac{(\Omega t)^4}{4!} + \frac{(\Omega t)^6}{6!} - \cdots\right)\hat{\omega}'^2 \\ &= I + \hat{\omega}' \sin\Omega t + \hat{\omega}'^2(1 - \cos\Omega t). \end{aligned} \quad (68)$$

Therefore

$$R(t) = \exp(\hat{\omega}t) = I + \hat{\omega}' \sin\Omega t + \hat{\omega}'^2(1 - \cos\Omega t). \quad (69)$$

ACKNOWLEDGMENTS

The authors thank Norden Systems, Northrop Grumman for providing X-band radar data for micro-Doppler analysis.

REFERENCES

[1] Gill, T. P.
The Doppler Effect, An Introduction to the Theory of the Effect.
Logos Press, Limited, 1965.

[2] Parker, K. J., Lerner, R. M., and Huang, S. R.
Method and apparatus for using Doppler modulation parameters for estimation of vibration amplitude.
U.S. Patent 5,086,775, Feb. 11, 1992.

[3] Zediker, M. S., Rice, R. R., and Hollister, J. H.
Method for extending range and sensitivity of a fiber optic micro-Doppler ladar system and apparatus therefore.
U.S. Patent 6,847,817, Dec. 8, 1998.

[4] Chen, V. C., and Ling, H.
Time-frequency transforms for radar imaging and signal analysis.
Boston, MA: Artech House, 2002, ch. 8.

[5] Censor, D.
Theory of the Doppler effect: Fact, fiction, and approximation.
Radio Science, **19**, 4 (1984), 1027–1040.

[6] Cooper, J.
Scattering of electromagnetic waves by a moving boundary: The one-dimensional case.
IEEE Transactions on Antennas and Propagation, **AP-28**, 6 (1980), 791–795.

[7] Cooper, J.
Scattering by moving bodies: The quasi-stationary approximation.
Mathematical Methods in the Applied Sciences, **2** (1980), 131–148.

[8] Kleinman, R. E., and Mack, R. B.
Scattering by linearly vibrating objects.
IEEE Transactions on Antennas and Propagation, **AP-27** (1979), 344–352.

[9] Van Bladel, J.
Electromagnetic fields in the presence of rotating bodies.
In *Proceedings of the IEEE*, **64**, 3 (1976), 301–318.

[10] Van Bladel, J., and De Zutter, D.
Reflections from linearly vibrating objects: Plane mirror at normal incidence.
IEEE Transactions on Antennas and Propagation, **AP-29** (1981), 629–636.

[11] De Zutter, D.
Reflection from linear vibrating objects: Plane mirror at oblique incidence.
IEEE Transactions on Antennas and Propagation, **AP-30** (1982), 898–903.

[12] Gray, J. E.
The Doppler spectrum of accelerating objects.
Presented at the IEEE International Radar Conference (Radar-90), May 1990.

[13] Gray, J. E., Conte, J. E., and Rice, T. R.
Target classification based on periodic motion characteristics.
In *Proceedings on the 2nd Automatic Target Recognizer Systems and Technology Conference*, vol. II, March 17–18, 1992.

[14] Gray, J.
The effect of non-uniform motion on the Doppler spectrum of scattered continuous wave waveform.
IEE Proceedings on Radar, Sonar and Navigation, **150**, 4 (2003), 262–270.

[15] Murray, R. M., Li, Z., and Sastry, S. S.
A Mathematical Introduction to Robotic Manipulation.
Boca Raton, FL: CRC Press, 1994.

[16] Cohen, L.
Generalized phase-space distribution functions.
Journal of Mathematical Physics, **7** (1966), 781–806.

[17] Cohen, L.
Time-Frequency Analysis.
Englewood Cliffs, NJ: Prentice-Hall, 1995.

[18] Qian, S., and Chen, D.
Introduction to Joint Time-Frequency Analysis—Methods and Applications.
Englewood Cliffs, NJ: Prentice-Hall, 1996.

[19] Chen, V. C., and Miceli, W. J.
Simulation of ISAR imaging of moving targets.
IEE Proceedings on Radar, Sonar and Navigation, **148**, 3 (2001), 160–166.

[20] Chen, V. C., Lipps, R., and Bottoms, M.
Advanced synthetic aperture radar imaging and feature analysis.
In *Proceedings of International Conference on Radar*, 2003, 22–29.

[21] Sparr, T., and Krane, B.
Micro-Doppler analysis of vibrating targets in SAR.
IEE Proceedings on Radar, Sonar and Navigation, **150**, 4 (2003), 277–283.

[22] Cutting, J., and Kozlowski, L.
Recognizing friends by their walk: Gait perception without familiarity cues.
Bulletin of the Psychonomic Society, **9** (1977), 353–356.

[23] Little, J. J., and Boyd, J. E.
Recognizing people by their gait: the shape of motion.
Journal of Computer Vision Research, **1**, 2 (1998).

[24] Niyogi, S. A., and Adelson, E. H.
Analyzing and recognizing walking figures in XYT.
IEEE Proceedings on Computer Vision and Pattern Recognition, (1994), 469–474.

[25] Lee, L., and Grimson, W. E. L.
Gait analysis for recognition and classification.
In *Proceedings of the 5th IEEE International Conference on Automatic Face and Gesture Recognition*, 2002, 148–155.

[26] Nixon, M. S., and Carter, J. N.
Advances in automatic gait recognition.
In *Proceedings of the 6th IEEE International Conference on Automatic Face and Gesture Recognition*, 2004, 139–144.

[27] Sabatini, A. M., and Colla, V.
A method for sonar based recognition of walking people.
Robotics and Autonomous Systems, **24** (1998), 117–126.

[28] Weir, R. F., and Childress, D. S.
A new method of characterizing gait using a potable, real-time, ultrasound ranging device.
In *Proceedings of the 19th International Conference*, IEEE Engineering in Medicine and Biology Society, 1997, 1810–1812.

[29] Chen, V. C.
Analysis of radar micro-Doppler signature with time-frequency transform.
In *Proceedings of the 10th IEEE Workshop on Statistical Signal and Array Processing*, 2000, 463–466.

[30] Geisheimer, J. L., Marshall, W. S., and Greneker, E.
A continuous-wave (CW) radar for gait analysis.
In *Proceedings of the 35th IEEE Asilomar Conference on Signal, Systems and Computers*, vol. 1, 2001, 834–838.

[31] Geisheimer, J. L., Greneker, E., and Marshall, W. S.
A high-resolution Doppler model of human gait.
Proceedings of SPIE on Radar Technology, 2002.

[32] van Dorp, P., and Groen, F. C. A.
Human walking estimation with radar.
IEE Proceedings on Radar, Sonar and Navigation, **150**, 5 (2003), 356–365.

Victor C. Chen received Ph.D. degree in electrical engineering from Case Western Reserve University, Cleveland, OH in 1989.

Since 1990 he has been with Radar Division, U.S. Naval Research Laboratory, Washington D.C., working on radar imaging, time-frequency applications to radar, ground moving target indication, and micro-Doppler analysis. He served as a technical representative he collaborating with several research groups in universities and monitored a number of Navy SBIR projects. As a project manager, he collaborates with international participants for an ONR NICOP S&T project. His current research interests include computational synthetic aperture radar imaging algorithms, time-frequency analysis for radar imaging and signal analysis, SAR GMTI, radar micro-Doppler analysis, and kernel machine/independent component analysis (ICA) for noncooperative target identification.

Dr. Chen serves as a program committee member and session chair for IEEE and SPIE conferences and served as a guest editor for *IEE Proceedings on Radar, Sonar and Navigation* in 2003, a guest editor for the *European Applied Signal Processing Journal* in 2005, and associate editor for *IEEE Transactions on Aerospace and Electronic Systems* since 2004. Dr. Chen received NRL Review Award in 1998, NRL Alan Berman Research Publication award in 2000 and 2004, and NRL Technical Transfer Award in 2002. He has more than 100 publications in books, journals, and proceedings including a book: *Time-Frequency Transforms for Radar Imaging and Signal Analysis* (V. C. Chen and Hao Ling), Artech House, Boston, MA, January 2002.

Fayin Li received the B.S. degree in automatic control from Huazhong University of Science and Technology, China, in 1996, and the M.S. degree in computer science from the Institute of Automation, Chinese Academy of Sciences, China, in 1999.

He is currently completing the Ph.D. degree in computer science at George Mason University, Fairfax, VA. His research interests include computer vision, machine learning, objects/location recognition, human-computer interaction, robotics, image processing, pattern recognition, and data mining. He is also interested in time-frequency analysis and its application.

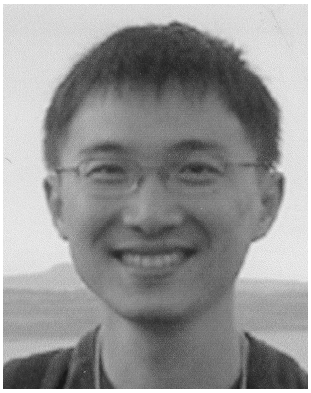

Shen-Shyang Ho received the B.Sc. degree in mathematics and computational science from the National University of Singapore, in 1999, the M.Sc. degree in computer science from George Mason University, 2003, and is currently pursuing Ph.D. degree in computer science from George Mason University.

His current interests include online learning from data streams, adaptive learning and pattern recognition.

Harry Wechsler (F'92) received the Ph.D. in computer science from the University of California, Irvine, in 1975.

Currently, he is a professor of computer science and director for the Center of Distributed and Intelligent Computation at George Mason University. His research in the field of intelligent systems focuses on computer vision, machine learning, and pattern recognition, with applications for active learning, biometrics/face recognition, clustering and concept drift/change, data mining, augmented cognition and intelligent HCI, performance evaluation, transduction, and video tracking and surveillance.

Dr. Wechsler has published more than 200 scientific papers and the book *Computational Vision* (Academic Press, 1990). As a leading researcher in face recognition, he organized the NATO Advanced Study Institute on "Face Recognition: From Theory to Applications" (1997), whose seminal proceedings were published by Springer (1998). He also directed the development and collection of FERET, which has become the standard facial data base for benchmark studies and experimentation. He was elected an IEEE fellow in 1992 for "contributions to spatial/spectral image representations and neural networks and their theoretical integration and application to human and machine perception"; and an IAPR (International Association of Pattern Recognition) fellow in 1998 for contributions to "computer vision and pattern recognition." He was granted (with his former doctoral students) two patents by USPO in 2004 on fractal image compression using quad-Q-learning and feature based classification (for face recognition).